

A&A manuscript no.

(will be inserted by hand later)

Your thesaurus codes are:

08 (02.13.1; 06.19.2; 08.06.2; 08.13.2; 09.10.1)

ASTRONOMY
AND
ASTROPHYSICS

Outflows from magnetic rotators

II. Asymptotic structure and collimation

T. Lery^{1,2}, J. Heyvaerts¹, S. Appl^{1,3}, and C.A. Norman⁴

¹ Observatoire de Strasbourg 11 rue de l'Université 67000 Strasbourg, France

² Department of Physics, Queen's University, Kingston, Ontario, K7L 3N6, Canada

³ Institut fuer Angewandte Mathematik, Universitaet Heidelberg, Im Neuenheimer Feld 293, D-69120 Heidelberg, Germany

⁴ Space Telescope Science Institute and Johns Hopkins University 3700 San Martin Drive, Baltimore, MD 21218, USA

Received 10 August 1998; accepted .

Abstract. The asymptotic structure of outflows from rotating magnetized objects confined by a uniform external pressure is calculated. The flow is assumed to be perfect MHD, polytropic, axisymmetric and stationary. The well known associated first integrals together with the confining external pressure determine the asymptotic structure. The integrals are provided by solving the flow physics for the base within the framework of the model developed in Paper I (Lery et al. 1998), which assumes conical geometry below the fast mode surface, transfield equilibrium being demanded only at the Alfvén surface, where it takes the form of the Alfvén regularity condition. This model can accept any set of boundary conditions. Its solutions are parameterized by the distribution with respect to flux of rotation rate $\Omega(a)$, specific entropy $Q(a)$ at the base of the jet, and by the mass to magnetic flux ratio on the polar axis α_0 . Having obtained the first integrals in the inner region, the external confining pressure enters as the only parameter of the asymptotic problem. We have taken it as independent of the distance to the wind source object, which results in an asymptotically cylindrical geometry. It is found that slow (i.e. with small rotation parameter ω) rigid rotators give rise to diffuse electric current distribution in the asymptotic region and are dominated by gas pressure. On the other hand, fast rigid rotators have a core-envelope structure in which a current carrying core is surrounded by an essentially current free region where the azimuthal magnetic field dominates. When the confining external pressure is made to decrease towards zero, the total asymptotic poloidal current carried in the wind zone decreases steadily, but does not seem to asymptote to a finite value for strictly zero outer pressure. A sizeable finite current remains present however for fast rotators even at exceedingly small, but still finite, pressure.

Key words: Magneto-hydrodynamics – Stars: pre-main

1. Introduction

Jets from young stellar objects (YSO) and active galactic nuclei (AGN) are most likely launched magnetically. Various approaches have been used to describe the stationary configuration of magnetically collimating winds governed by the Grad-Shafranov equation (e.g. Lery et al. 1998 hereafter Paper I, and references therein). Magnetized rotating MHD winds can be accelerated from an accretion disk (“Disk wind”, Blandford & Payne 1982, Pelletier & Pudritz 1992), at the disk-magnetosphere boundary (“X-winds”, Shu et al. 1988, 1994) or directly from the star itself by combined pressure and magneto-centrifugal forces (“Stellar wind”, Weber & Davis 1967, MacGregor 1996 and reference therein). In order to make the system of equation more tractable angular self-similarity has been often employed for non rotating magnetospheres (Tsinganos & Sauty 1992), and outflows from spherical rotating objects (Sauty & Tsinganos 1994, Trussoni et al. (1997), Tsinganos et Trussoni 1991). Cylindrical self-similarity has also been used for magnetized jets (Chan & Henriksen 1982), and spherical self-similarity for disk winds (Blandford & Payne 1982, Henriksen & Valls-Gabaud 1994, Fiege & Henriksen 1996, Contopoulos & Lovelace 1994, Ferreira & Pelletier 1993, Ferreira 1997). However this assumption presents boundary condition restrictions. Several numerical simulations, such as Ouyed & Pudritz 1997, have been made in order to understand the formation of magnetized jets from keplerian discs, but due to computational limitations only a few cases have been studied. One should also note that pure hydrodynamic collimation could be effective at producing jets (Frank & Mellema 1996). High velocity outflows from YSO and AGN are observed to be highly collimated. Heyvaerts & Norman (1989) have discussed how streamlines asymptotically develop in winds with different properties without considering confinement by any external medium (see also

other winds focus parabolically. Li et al. (1992) showed how the formation of weakly collimated, conical flows depends on the shape of the poloidal field near the Alfvén surface. The transition from weakly collimated flows to highly collimated jets has been also studied by Sauty & Tsinganos (1994).

In Paper I we have proposed a model for the stationary structure of the inner part of the flow, close to the emitting object, based on the assumption that the magnetic surfaces possess a shape which is a priori known inside the fast critical surface. As a first approximation magnetic surfaces were taken to be cones. Unlike the Weber-Davis type models, the balance of forces perpendicular to the magnetic surfaces is taken into account on the Alfvénic surface through the Alfvén regularity condition. This, together with the criticality conditions determine the three unknown constants of the motion, that are conserved along magnetic surfaces a , namely the specific energy $E(a)$, the specific angular momentum $L(a)$ and the mass to magnetic flux ratio $\alpha(a)$. Once these first integrals are determined, the asymptotic cylindrically collimated flow is uniquely determined. The solutions are parameterized by the angular velocity of the magnetic field lines $\Omega(a)$, the specific entropy at the base $Q(a)$ and by the mass flux to magnetic flux ratio on the polar axis α_0 . According to the rotation parameter $\omega = \frac{\Omega r_A}{v_{PA}}$ the objects can be classified as slow ($\omega \ll 1$), fast ($((\frac{3}{2})^{3/2} - \omega \ll 1)$) or intermediate (other values of ω ranging between 0 and $(\frac{3}{2})^{3/2}$) rotators. Critical surfaces are nearly spherical for slow rotators, but become strongly distorted for rapid rotators, giving rise to important gradients of density and velocity that should consequently effect asymptotic quantities. This simplified model makes it possible to investigate the structure of outflows far from the magnetized rotator source without the need for self-similar assumptions. The price to pay for that is that the model does not give an exact, but only an approximate, solution because the transfield equation is not solved everywhere, but only at a few special places.

How outflows behave in the asymptotic region constitutes the subject of the study of this paper which also focuses on the study of the asymptotic electric current and addresses the question of the asymptotic collimation of the different classes of rotators found in Paper I. In this paper, we present a model where the collimated jet is assumed to be in pressure equilibrium with an external medium whose properties are independent of the distance to the source. The question of the asymptotic electric current is a major concern for jets that will be investigated.

We structure our paper as follows: In §2, we present the equations governing the asymptotic equilibrium, their boundary conditions and the numerical method we use.

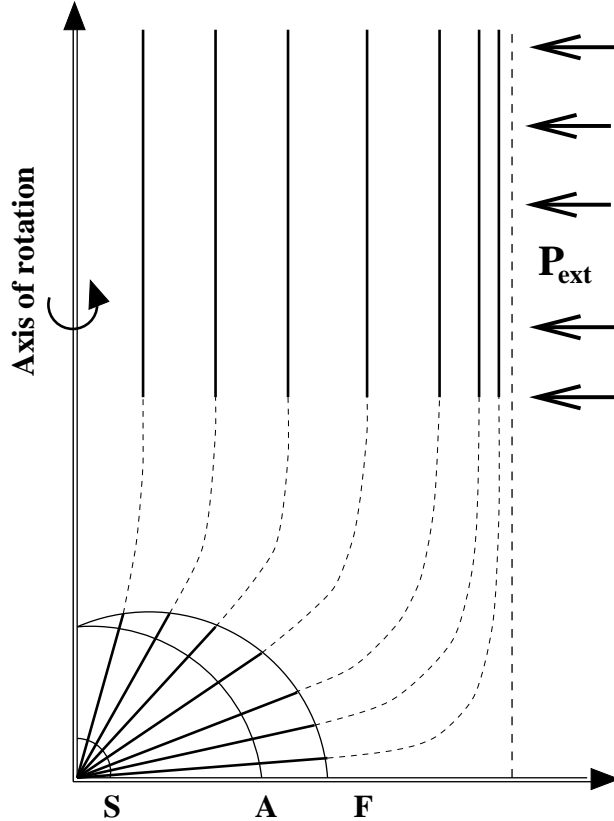


Fig. 1. Schematic representation of the magnetic structure of the model. The magnetic surfaces projected in the poloidal plane are conical within the fast magnetosonic surface and connect to the cylindrical asymptotic region. In this part, the outflow is surrounded by an external confining medium. S, A and F denote the slow magnetosonic, the Alfvén and the fast magnetosonic surfaces, respectively.

implications of our analysis and we summarize our results in §6.

2. The collimated jet

2.1. The jet base

We study the stationary structure of a magnetized jet in pressure equilibrium with the ambient medium. The flow is described by ideal magnetohydrodynamics. Magnetic surfaces are assumed to be still conical at the fast magnetosonic surface, and eventually become cylindrical due to confinement by uniform external pressure (Fig.1). We work in the cylindrical coordinate system (r, ϕ, z) whose axis coincides with the symmetry-axis. Each flux surface is labeled by the flux function $a(r, z)$ proportional to the magnetic flux through a circle centered on the axis passing at point r, z . The physical flux is $2\pi a$. The equatorial

flow to be related to the gas pressure P by a polytropic equation of state

$$P = Q(a)\rho^\gamma. \quad (1)$$

We refer to $Q(a)$ as the "specific entropy" of the flow, though it would be related to it only for adiabatic flows. The constant γ is the polytropic index which is considered to be constant. The specific entropy $Q(a)$, the angular velocity of the magnetic field lines $\Omega(a)$ and the mass to magnetic flux ratio are constant along any flux surface a . Also, $\alpha(a)$ equals α_0 all along the polar line. The functions $Q(a)$, $\Omega(a)$ and the parameter α_0 entirely determine the outflow in the conical region. The total energy $E(a)$, the total angular momentum $L(a)$, and the ratio of matter to magnetic flux $\alpha(a)$, expressed through the density at the Alfvén point $\rho_A(a)$, are also conserved along the flux surfaces and follow from the regularity of the solution at the Alfvénic and fast and slow magnetosonic surface. For the details, as well as for the meaning of the symbols, we refer to paper I. The MHD flow in regions causally disconnected from the base region has no back-reaction on its properties in this region. It is known that this causally disconnected region starts at the so-called fast limiting characteristic (Tsinganos et al. 1996), which is usually situated downflow from the fast magnetosonic surface. The flow in the causally disconnected region has no influence on the values assumed by the three first integrals which are not a-priori known. The flow between the fast mode critical surface and the fast mode limiting separatrix would have some influence on their determination if the shape of magnetic surfaces between the source object and the fast limiting separatrix were self-consistently calculated by solving exactly the transfield equation. However, in the simplified and fixed base geometry of our model, these first integrals are entirely determined from sub-fast surface regions and there is no need, for their determination, nor for that of the asymptotic structure, to calculate the geometry of magnetic surfaces in the intermediate region between the fast critical surface and the fast mode limiting separatrix. The latter is anyway presumably located not much further away from it and we do not expect large geometrical changes as compared to the base region. The lack of complete self-consistency of our model is therefore mainly contained in our assumption of base conical geometry. The fact that the shape of surfaces is not calculated downflow from the fast surface in regions where field curvature is still present, i.e. where poloidal field lines are dashed in Fig.1, does not add any supplementary inaccuracy.

The shape of the magnetic surfaces shown in Fig.1 are similar, to some extent, to shapes obtained by some previous studies already performed for a self-consistent calculation of the shape of the poloidal field lines. Trussoni et al. (1997) have prescribed similar types of the magnetic

constant polytropic index γ . Sauty and Tsinganos (1994) have also calculated the shape of magnetic field lines by deducing them and integrating the MHD equations from the base to large distances.

2.2. Equations for the asymptotic structure

The asymptotic structure of the flow is determined by the Bernoulli equation and the force balance in the direction perpendicular to the field (transfield equation) in terms of the constants of motion Q, Ω, E, L, α . Bernoulli equation can be written as:

$$\frac{1}{2} \frac{\alpha^2 \nabla a^2}{\rho^2 r^2} = E(a) - G(r, z) - \frac{\gamma}{\gamma - 1} Q \rho^{\gamma-1} + \rho \Omega \frac{L - r^2 \Omega}{\rho_A - \rho} - \frac{1}{2} \left(\frac{L}{r} + \frac{\rho}{r} \frac{L - r^2 \Omega}{\rho_A - \rho} \right)^2, \quad (2)$$

where $G(r, z)$ is the gravitational potential, L the total angular momentum, and ρ_A the mass density at the Alfvén critical point. The Bernoulli equation can be simplified in the asymptotic region, i.e. z going to ∞ , so that gravity becomes negligible. In the cylindrical case, ∇a is replaced by da/dr . Since we are far from the Alfvén surface in the asymptotic region, the density of the flow ρ must be smaller than the Alfvénic density ρ_A . Moreover we can consider r to be larger than r_A . Using the assumptions $r \gg r_A$ and $\rho_A \gg \rho$, the last two terms of the Eq. (2) become:

$$- \frac{\rho \Omega^2 r^2}{\rho_A} - \frac{1}{2} \frac{r_A^4 \Omega^2}{r^2} \left[1 - \frac{\rho r^2}{\rho_A r_A^2} \right]^2. \quad (3)$$

This is equivalent to:

$$- \frac{\rho \Omega^2 r^2}{\rho_A} - \frac{\rho \Omega^2 r^2}{\rho_A} \left[\frac{1}{2} \left(\frac{\rho_A r_A^2}{\rho r^2} \right) \frac{r_A^2}{r^2} - \frac{r_A^2}{r^2} + \frac{1}{2} \frac{\rho}{\rho_A} \right]. \quad (4)$$

The last two terms in brackets are negligible w.r.t. unity. Moreover when z tends to infinity, ρr^2 is bounded. Therefore the parenthesis of the first term inside the brackets is also bounded, and, if r were to approach infinity, the first term in bracket would also be negligible with respect to unity. We assume that, even though r approaches a finite limit, (r_A/r) becomes asymptotically small enough for this first term in bracket to also become negligible. Thus the last two terms of Bernoulli equation can be approximated at infinity by:

$$- \frac{\rho \Omega^2 r^2}{\rho_A}. \quad (5)$$

Bernoulli equation now becomes

$$\frac{1}{2} \left(\frac{\alpha}{\rho r} \frac{da}{dr} \right)^2 = E - \frac{\gamma}{(\gamma - 1)} Q \rho^{(\gamma-1)} - \frac{\Omega^2 r^2 \rho}{\mu_0 \alpha^2}. \quad (6)$$

The transfield equation can be written in cylindrical co-

$$= E' - \frac{Q' \rho^{\gamma-1}}{\gamma-1} + \frac{\alpha'}{\alpha} \frac{\mu_0 \alpha^2 \rho}{r^2} \frac{(L - r^2 \Omega)^2}{(\mu_0 \alpha^2 - \rho)^2} - \frac{\rho}{r^2} \frac{(L' - r^2 \Omega')(L - r^2 \Omega)}{\mu_0 \alpha^2 - \rho} - \frac{L L'}{r^2}.$$

Primes denote derivatives with respect to a , i.e. $E' = dE/da$. Similarly using the same asymptotic assumptions in the transfield equation, the centrifugal force $\rho v_\phi^2/r$ can be neglected with respect to “hoop stress” $B_\phi^2/\mu_0 r$ since

$$\frac{\rho v_\phi^2}{r} = \frac{B_\phi^2}{\mu_0 r} \left(\frac{r_A^2}{r^2} \right) \left(\frac{\rho A r_A^2}{\rho r^2} \right) \left(1 - \frac{\rho r^2}{\rho A r_A^2} \right)^2. \quad (8)$$

Hence due to the simplifications, several force densities vanish in the one-dimensional form of transfield equation that is then given by:

$$\frac{1}{2} \frac{d}{da} \left(\frac{\alpha}{\rho r} \frac{da}{dr} \right)^2 = E' - \frac{1}{\gamma-1} Q' \rho^{\gamma-1} + \frac{\rho r^2 \Omega^2}{\mu_0 \alpha^2} \left(\frac{\alpha'}{\alpha} - \frac{\Omega'}{\Omega} \right). \quad (9)$$

Subtracting the transfield equation (9) from the derivative with respect to a of the Bernoulli equation (6), one can simplify the transfield equation that becomes:

$$r^2 \frac{d}{da} (Q \rho^\gamma) + \frac{1}{2} \frac{d}{da} \left(\frac{\Omega^2 r^4 \rho^2}{\mu_0 \alpha^2} \right) = 0. \quad (10)$$

Thus equations (6) and (10) describe the asymptotic equilibrium structure of a magnetized jet with the present assumptions. To study the equilibrium of this jet taking into account an external ambient pressure, one needs to specify the relevant boundary condition at the jet's edge.

It is possible to show that the asymptotic problem with non-vanishing external pressure does not accept solutions where r goes to infinity on any magnetic field line. Indeed, if so, $\frac{da}{dr}$ would vanish at the edge of the jet. As a consequence $B_p = \frac{1}{r} \frac{da}{dr}$ would go to zero at the outer edge and the toroidal part of the magnetic field would asymptotically reduce to

$$B_\phi = \mu_0 \alpha \frac{\rho}{\rho_A - \rho} \frac{L - r^2 \Omega}{r} \approx -\frac{\Omega}{\alpha} \frac{\rho r^2}{r} \quad (11)$$

If ρr^2 were to diverge at the edge, the Bernoulli equation (equation (2)) would be violated, since the left hand side term is always positive, and the ninth term that is negative and the largest one in absolute value could not be balanced by other terms. It would also be so if the Alfvén radius were to become infinite. This proves that B_ϕ and B_p should vanish if r were to approach infinity. If so, the boundary condition reduces to:

$$P_{ext} = P_{gas} = Q \rho_b^\gamma. \quad (12)$$

The density at the outer edge ρ_b would then be finite, and ρr^2 would diverge which violates the Bernoulli equation

Let us see now that the physics of the flow in the inner region close to the source constrains the maximum value of the asymptotic mass density on the polar axis, ρ_0 , and therefore also the total mass flux for a given magnetic flux. Indeed, on the axis the Bernoulli equation reduces to

$$\left(\frac{1}{2} v_P^2 \right) = E - \frac{\gamma}{\gamma-1} Q \rho_0^{\gamma-1}. \quad (13)$$

which yields an upper limit to the axial density (the limit corresponding to a vanishing asymptotic poloidal velocity),

$$\rho_0 \leq \left(\frac{\gamma-1}{\gamma} \frac{E}{Q} \right)^{\frac{1}{\gamma-1}}. \quad (14)$$

In the inner region of the flow close to the source the energy has been calculated (see paper I). For slow rotators (that corresponds to a rotation parameter $\omega \ll 1$) energy is given by

$$E = \frac{A^2}{2 \mu_0^2 \alpha^2 R_A^4} \quad (15)$$

with the Alfvén spherical radius equal to:

$$R_A = \left(\frac{C_1 \mu_0 A^2}{2} \right)^{\frac{1}{2(\sqrt{2}+2)}} \quad (16)$$

where C_1 is the constant of integration of the transfield equation that has been defined analytically in Paper I (equation (75)) only as a function of the input parameters. Combining the two last equations with equation (14) the maximum density becomes in this case

$$\rho_{0,\max} = \left(\frac{\gamma-1}{\gamma} \frac{A^2}{2 \mu_0^2 \alpha^2 Q} \left(\frac{2}{C_1 \mu_0 A^2} \right)^{\frac{2}{\sqrt{2}+2}} \right)^{\frac{1}{\gamma-1}}. \quad (17)$$

In the vanishing rotation case, it is then possible to find an analytical definition of the maximum density on the axis in the asymptotic region allowed by the input parameters defining the emitting source properties. This also shows that the slow rotator limiting density essentially depends on the specific entropy Q . For fast rotators and using equation (99) of Paper I that gives energy, the limiting mass density becomes

$$\rho_{0,\max} = \left(\frac{\gamma-1}{\gamma} \frac{3}{2Q} \frac{A \Omega^2}{\mu_0 \alpha} \right)^{\frac{1}{\gamma-1}}. \quad (18)$$

This limit now depends on the entropy, but also on angular velocity and mass to magnetic flux ratio. The latter parameter is related to mass loss rate on the axis and therefore determine the axial value of density at the Alfvén point. Then an increase of α_0 naturally reduces this limit.

smaller than this limit. It will only depend on the pressure of material surrounding the outflow since we further assume the flow to be in pressure equilibrium with an external medium whose pressure is constant. Equilibrium at the jet boundary is expressed by

$$P_{\text{ext}} = Q\rho^\gamma + (B_P^2 + B_\phi^2)/(2\mu_0), \quad (19)$$

with the magnetic contributions

$$\frac{B_\phi^2}{2\mu_0} = \frac{\rho^2 r^2 \Omega^2}{2\rho_A}, \quad (20)$$

$$\frac{B_P^2}{2\mu_0} = \frac{\rho^2}{\rho_A} \left(E - \frac{\gamma}{\gamma-1} Q\rho^{\gamma-1} - \frac{\Omega^2 r^2 \rho}{\rho_A} \right). \quad (21)$$

It has been used that at the outer boundary $\rho \ll \rho_A$ and $r \gg r_A$. The pressure of the external medium may have a thermal and a magnetic contribution, too. In the case of a finite external pressure the jet radius remains finite.

Thus transfield and Bernoulli equations in their asymptotic forms and the pressure balance at the outer edge constitute the set of equations describing the asymptotic structure of the pressure-confined jet. The three first integrals of the motion $E(a)$, $L(a)$ and $\alpha(a)$ are obtained from the inner part of the flow (Paper I). At infinity the only free parameter is the external pressure P_{ext} .

2.3. Numerical procedure

For the numerical calculations, Bernoulli and transfield equations have been reformulated as two ODEs for the radial position, r , and the density, ρ , as a function of the flux surfaces a . The Bernoulli equation can be written as:

$$\frac{dr}{da} = \frac{\alpha}{\rho r \sqrt{2} \sqrt{E - \frac{\gamma}{\gamma-1} Q\rho^{\gamma-1} - \frac{\Omega^2 r^2 \rho}{\mu_0 \alpha^2}}} \quad (22)$$

and the transfield equation can be written as

$$\begin{aligned} \left(\mu_0 \gamma Q \rho^{\gamma-2} + \frac{r^2 \Omega^2}{\mu_0 \alpha^2} \right) \frac{1}{\rho} \frac{d\rho}{da} + \left(\frac{2r\Omega^2}{\mu_0 \alpha^2} \right) \frac{dr}{da} \\ = \frac{r^2 \Omega^2}{\mu_0 \alpha^3} \frac{d\alpha}{da} - \mu_0 \rho^{\gamma-2} \frac{dQ}{da} - \frac{r^2 \Omega^2}{\mu_0 \alpha^2} \frac{d\Omega}{da}. \end{aligned} \quad (23)$$

These two equations can now be written symbolically as

$$\frac{dr}{da} = f_r(r, \rho, E, Q, \alpha, \dots), \quad (24)$$

$$\frac{d\rho}{da} = f_\rho(r, \rho, E, Q, \alpha, \dots), \quad (25)$$

where f_r is the r.h.s. of equation (22) and f_ρ has a more complex form that can be easily derived from equations (23) and (22). We use an initial conditions standard integrators for stiff systems of first order ordinary differential equations (ODE). We then prescribe the axial density

for Ω , α_0 and Q in order to simplify numerical investigations. The reference units (in CGS) are $\rho_{\text{ref}} = 70 p.cm^{-3}$, $r_{\text{ref}} = 10^{15} cm$, $v_{\text{ref}} = 10^7 cm.s^{-1}$. In the following we present solutions for the jet equilibrium, equations. (22, 23), subject to equilibrium with a surrounding medium at constant pressure. We study the behavior of the solutions as a function of specific rotation Ω and specific entropy Q of the central object. The integrals of motion are obtained as described in paper I.

3. Constant rotation

We now consider the case of magnetized winds originating from objects with constant rotation and entropy. The effect of the four parameters, Ω_* , Q_* , $\alpha_{0,*}$, and P_{ext} is studied in the next subsections, followed by a specific application to the TTauri star BP Tau.

3.1. Variations of rotation

First we study the effect of the dimensionless angular velocity, $\bar{\Omega}(a) = \Omega_*$ of the central object leaving the specific entropy constant, $\bar{Q} = Q_*$, as well as the mass-to-magnetic flux ratio on the axis, $\bar{\alpha}_0$, and the external pressure, P_{ext} . As in paper I we discuss the different regimes in terms of slow and fast rotators.

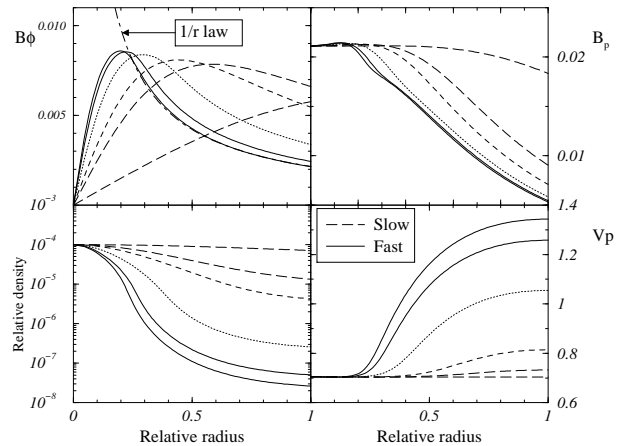


Fig. 2. The azimuthal B_ϕ and poloidal B_P magnetic field components (upper left and right panels respectively), density ρ and poloidal velocity v_P (lower left and right panels) are plotted as functions of relative radius r_{rel} for different values of the dimensionless rotation rate $\bar{\Omega}$ which varies from $\bar{\Omega} = 2$ (dashed lines) to $\bar{\Omega} = 11$ (solid lines) with $\bar{\Omega} = 4, 6, 8, 10$ as intermediate values. $\bar{Q} = 2.1$ and $\bar{\alpha}_0 = 1.7$. The corresponding values of ω are 0.4, 1.1, 1.3, 1.65, 1.75 and 1.8.

In paper I we have found that the variations of the

For the other parameter we chose $Q_* = 2.1$. The various curves the correspond to $\bar{\alpha} = 1.7$.

In a slow rotator (heavy dashed lines in Fig.2) the toroidal field increases nearly linearly, while for jets from fast rotators it possesses a maximum within the jet, and then falls off as $\propto 1/r$ while $B_p \propto 1/r^2$. This corresponds to a diffuse current with nearly constant current density, or a centrally peaked current, surrounded by a current-free envelope, respectively. This will be discussed in more detail in Sect. 5. A similar behavior has been discussed by Appl & Camenzind (1993) for relativistic jets, according to which the jet configurations had been referred to as diffuse and sharp pinch. Important variations with respect to rotation can also be seen in the other physical quantities. In particular the poloidal velocity is highest in the envelope, though variations remain within a factor of two. In the very fast rotator limit the density falls off dramatically in the envelope where the gas pressure becomes negligible compared to the magnetic pressure. This is clearly shown in Fig.(3) where the total pressure is represented with magnetic and gas pressures. For slow rotators, the

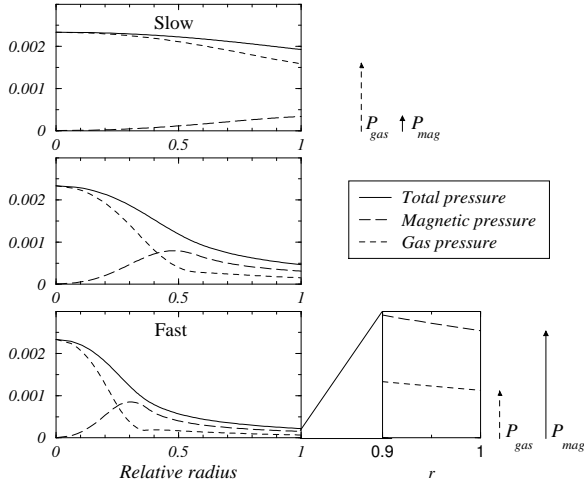


Fig. 3. Comparison of pressure profiles for slow, fast and very fast rotators. Total, magnetic (P_{mag}) and gas (P_{gas}) pressure respectively correspond to solid, dashed and long dashed lines. The rotation parameter ω is equal to 0.4, 1.3 and 1.8 top to bottom respectively.

gas pressure dominates everywhere in the outflow, while for fast rotators the magnetic pressure dominates in the envelope. Fig.(4) shows the variation of ρ_b as a function of the parameter ω . Most of the outer pressure at the outer edge is supported by magnetic field and not by gas pressure. This effect is very effective for very fast rotators.

In Fig.(5), the mass to magnetic flux ratio $\bar{\alpha}$ is represented as a function of the relative magnetic flux for

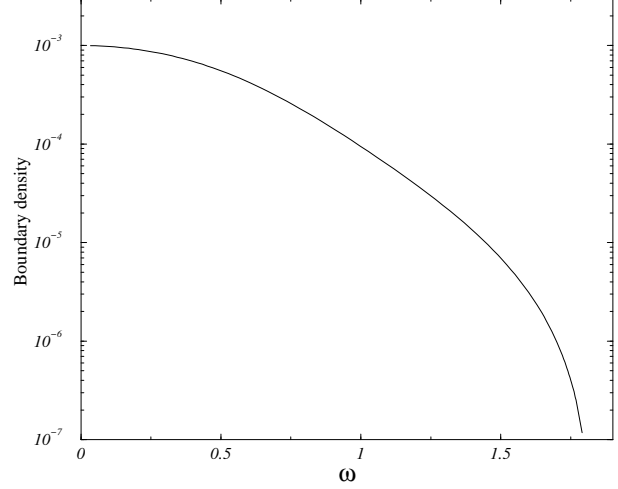


Fig. 4. Density ρ_b at the outer edge of the jet as a function of the rotation parameter ω which varies from 0 to its maximum value $(\frac{3}{2})^{3/2}$. The density on the axis ρ_0 remains the same for all the solutions.

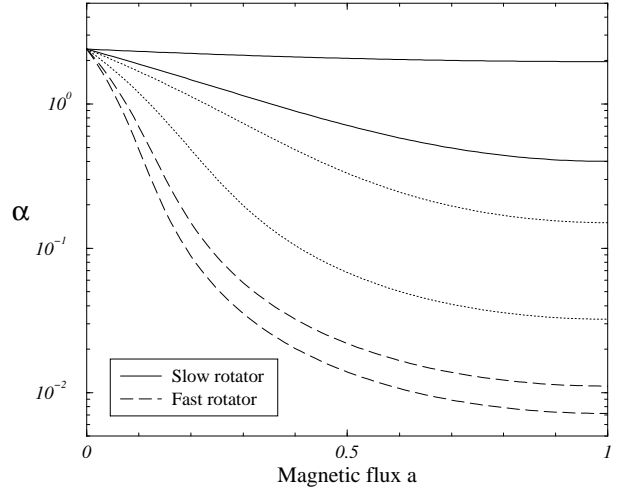


Fig. 5. Plot of the mass to magnetic flux ratio $\bar{\alpha}$ with respect to the relative magnetic flux $a_* = \frac{a}{A}$ for various constant rotation rates $\bar{\Omega} = 2..11$. Solid lines correspond to slow rotators, and long dashed lines to outflows with large $\bar{\Omega}$. All the other parameters and boundary conditions are kept the same.

It means that most of the matter is flowing along the polar axis for fast rotators.

Thus slow rotators generally have smaller variations of the physical quantities across the jet than fast rotators. The latter are characterized by a dense, current-carrying

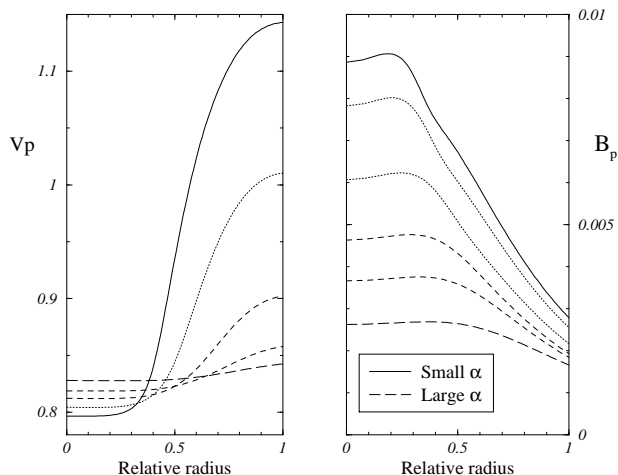


Fig. 6. Plots of poloidal components of velocity v_p (left panel) and magnetic field B_p (right panel) for various values of the mass to magnetic flux ratio on the axis $\bar{\alpha}_0$. Heavy solid line correspond to small mass loss rates and heavy dashed line to large ones. ($\bar{\alpha}_0 = 0.7, 0.8, 1, 1.4, 1.8, 2.6$, $\bar{\Omega} = 5$ and $\bar{Q} = 2.5$)

3.2. Mass loss rate

Another potentially observable quantity is the mass loss rate particularly interesting since it can be evaluated from observations. The parameter related to the mass loss rate is $\bar{\alpha}_0$, the mass to magnetic flux ratio on the polar axis. We have computed solutions for different $\bar{\alpha}_0$'s, keeping other parameters unchanged. The results are plotted in Fig.(6) where the poloidal components of velocity v_p and magnetic field B_p are represented as functions of the relative radius. The input values are $\bar{\alpha}_0 = 0.7, 0.8, 1, 1.4, 1.8, 2.6$, $\bar{\Omega} = 5$ and $\bar{Q} = 2.5$. Since the density always decreases from the axis to the outer edge the poloidal velocity allows to locate the region of maximum momentum, the central part for most cases, especially for fast rotators. When the mass loss rate grows, the outflow is slowed down on the edge and accelerated on the axis, while the poloidal magnetic field is also reduced. The profile of poloidal velocity depends sensitively on $\bar{\alpha}_0$ as well as the core radius that reduces as $\bar{\alpha}_0$ increases. As found in Paper I for the inner conical region, it appears that an increase in mass loss rate has a similar effect to a decrease of the rotation rate. For small ejection rates the poloidal magnetic field possesses its maximum not on the axis.

3.3. Thermal effects

In this subsection we study the dependence of the outflow properties on specific entropy Q , on the stellar surface

calculated at the outer edge of the flow as functions of the specific entropy \bar{Q} . The whole range in ω can be covered by only varying \bar{Q} . Smaller specific entropies correspond to larger ω . For given $\bar{\Omega}$ and $\bar{\alpha}_0$ the poloidal velocity presents a minimum when the rotation parameter ω is almost equal to unity which corresponds to the intermediate class of rotators. Slow rotators are then accelerated by an increase of the heating, but not fast rotators. It has also been found that a change in specific entropy does not affect the azimuthal to poloidal magnetic field ratio but just produces an increase of magnitudes.

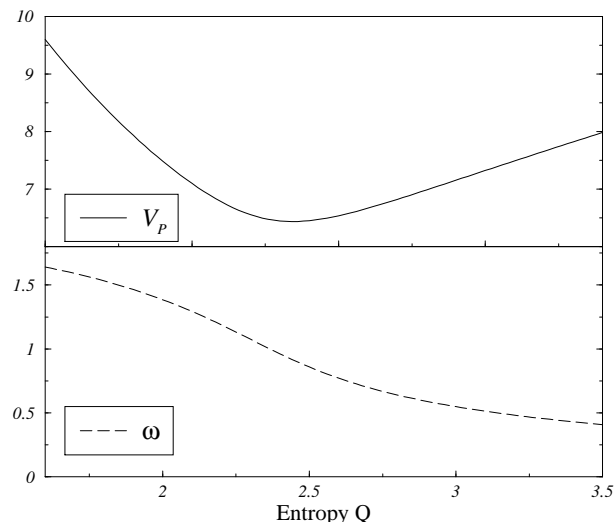


Fig. 7. Poloidal velocity v_p (upper panel) and rotation parameter ω (lower panel) are plotted for \bar{Q} varying from 1.2 to 3.5 given at the boundary of the outflow. ω varies from 0 to its maximum value. $\bar{\Omega} = \Omega_* = 5$, $\bar{\alpha}_0 = 2.1$ and $\rho_0 = 10^{-5}$.

In Fig.(8), the combined effects of \bar{Q} and γ are represented. The rotation parameter ω is plotted with respect to γ for various values of \bar{Q} . Two different classes of solutions can be distinguished, solutions for which ω start at small values for $\gamma = 1$ and then decrease and solutions which have large ω at $\gamma = 1$ and then increase. Thus the value of the specific entropy discriminates between fast and slow rotators while larger γ 's just tighten this distinction.

The variation of the poloidal velocity v_p calculated at the boundary of the outflow is shown in Fig.(9) as a function of γ for a fast rotator. The velocity is seen to change by three orders of magnitude, between the isothermal and adiabatic flow showing the whole possible range of variations of the parameter. The kinematics of the jet is therefore rather sensitive to heating or cooling of the jet. More-

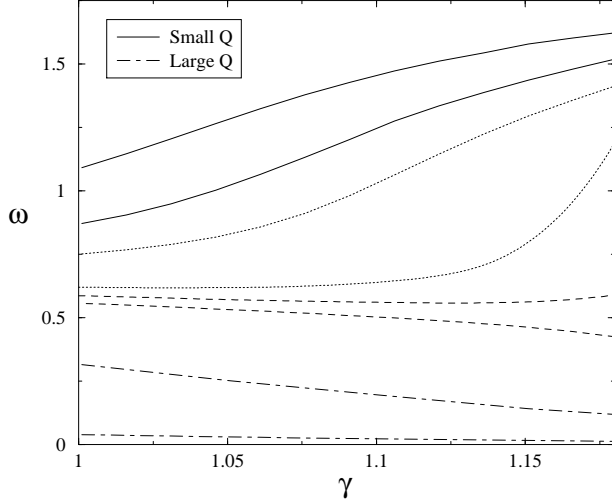


Fig. 8. The rotation parameter ω given at the outer boundary as a function of γ for different values of \bar{Q} (from 1 to 3.5). The smallest values of \bar{Q} (represented with solid lines) increase and reach the largest value of ω , while larger value of \bar{Q} (dashed lines) decrease and correspond to smaller values of ω .

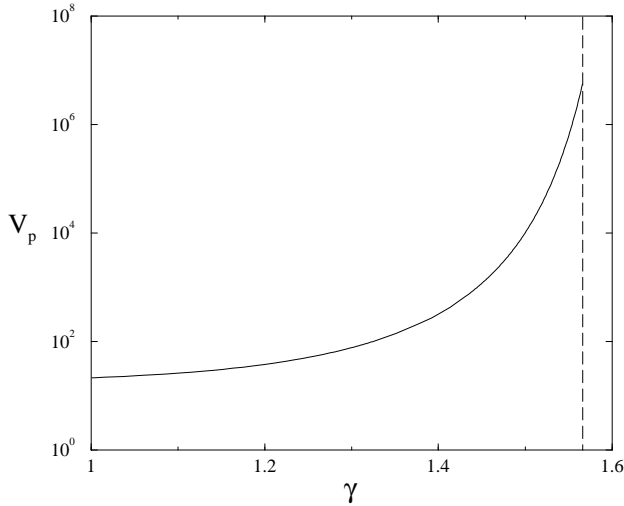


Fig. 9. Plot of the poloidal velocity v_p calculated at the outer edge of the outflow as a function of the polytropic index γ which varies from 1 (isothermal case) to its maximum value $\frac{5}{3}$.

3.4. The external pressure

At the outer edge of the outflow, the value of the external pressure is prescribed as a boundary condition. Since we prefer for numerical convenience to use initial condition solver for the integration of our system of equations we prescribe the axial density rather than the external pres-

sure. As the poloidal velocity increases, two. Note, however, that even for a strong variation of the external pressure, the velocity is not affected very much. Nevertheless denser jets appear to be slower at the boundary than more tenuous ones.

3.5. An example: BP Tau

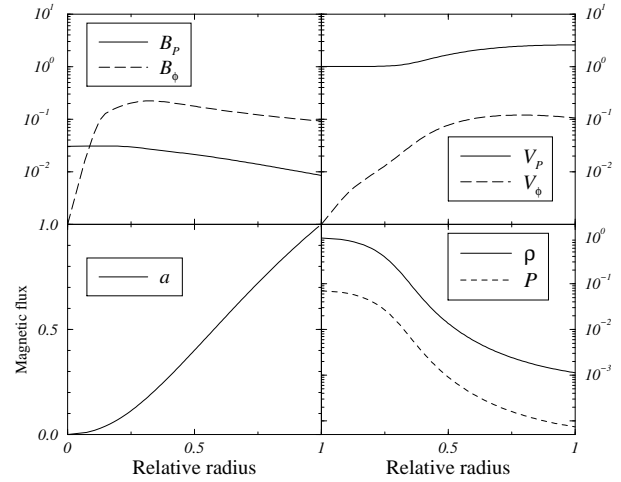


Fig. 10. Model for the jet of a T Tauri star, BP Tau with $\bar{\Omega} = 1.8$, $\bar{\alpha}_0 = 0.1$, $\bar{Q} = 0.05$ and a relative central density of 10^{-4} . $\bar{\Omega}$ and \bar{Q} are constant across the jet. The deduced rotation parameter ω is equal to 1.41. Upper panels correspond to Magnetic field (left) and velocity components (right). Density and gas pressure (right) together with the relative magnetic flux (left) are represented in the lower panels as a function of the relative radius $r_{rel} = \frac{r}{r_{jet}}$.

We now apply the stellar jet model to the T Tauri star BP Tau. Bertout et al.(1988) give for the properties of this star the following values: $\dot{M}_* = 2 \times 10^{-7} M_\odot \text{yr}^{-1}$, $M_* = 0.8 M_\odot$, $R_* = 3 R_\odot$, $T_* = 9 \times 10^3$, $n_p = 10^4 \text{cm}^{-3}$, and $B_* = 1000 \text{G}$. On the base of these values we deduce (see paper I) the corresponding input parameters, which are, expressed in terms of the dimensionless reference values mentioned in section 2.3: $\bar{Q} = 0.05$, $\bar{\Omega} = 1.8$, $\bar{\alpha}_0 = 0.1$ and a relative central density of 10^{-4} . These parameters allow to compute the dimensionless rotation parameter ω which is found to be 1.41 on the equator, and corresponds to the case of a fast rotator. Magnetic field and velocity components, density and gas pressure in the flow are plotted for BP Tau in Fig.(10) together with the magnetic flux represented as a function of the relative radius. The reference units (in CGS) are $\rho_{ref} = 70 \text{p.cm}^{-3}$, $r_{ref} = 10^{15} \text{cm}$, $v_{ref} = 10^7 \text{cm.s}^{-1}$.

The azimuthal component of the magnetic field domi-

strong variation across the jet, and the azimuthal velocity v_ϕ is one order of magnitude smaller than the poloidal component. The maximum poloidal velocity correspond to the minimum of density. Density and gas pressure vary by 3 order of magnitudes from polar axis to edge. The axial region is the densest and slowest part of the asymptotic flow. This dense core region is a fraction of the full jet with a minimum of 0.5 for the fastest case. This corresponds to a central core of the order of $5 \times 10^{14} \text{ cm}$. Even if the fastest part is the outer one the maximum momentum is located around the polar axis. This way the central part of the flow will penetrate more easily the ambient medium during the propagation of the jet, the outer region of the outflow being slowed down. Thus even if the relative velocity is smaller close to the axis the central region of the flow will propagate faster.

Moreover the kinetic to Poynting flux ratio can be calculated as a function of the relative radius. It is found that only in the central part of the asymptotic outflow does the kinetic energy flux dominate over Poynting flux. It shows that a large part of the magnetic energy has not been transferred to the kinetic energy in the case of constant rotation.

3.6. Summary

In this section we have investigated the asymptotic jet properties for outflows from rigidly rotating stellar objects with constant entropy. The classification given in Paper I between slow and fast rotators is still valid since the variables ω, α, E, Q and Ω are defined in the inner region and are not affected by values of the external pressure. We have studied the influence of the rotation parameter. For slow and fast rotators, with $0 \leq \omega \leq (\frac{3}{2})^{3/2}$ and for γ running from 1 to $\frac{5}{3}$ the solutions obtained exhibit large gradients of density and pressures in jets from fast rotators. These correspond to either cold outflows, fast rotation or low mass loss rate. They exhibit a concentrated azimuthal magnetic field B_ϕ , have a smaller mass flux and have strong density gradients. The envelope is dominated by magnetic pressure, while the core, similarly to slow rotators, is gas pressure dominated.

4. Non-constant Ω and Q

The question of profiles of angular velocity and specific entropy has to be assessed because real astrophysical objects do not possess constant values of these two functions from the axis to the outer edge. For example the rotation of the sun is known to be differential and in the case of young stellar objects some part of the outflow come from a disk characterized by differential rotation with strong radial variations of density and temperature.

zero with a step-like transition, the same for Ω_3 but more smoothly, Ω_2 and Ω_5 vary from Ω_0 to $\Omega_0/2$ and $1.5 \times \Omega_0$ respectively and finally Ω_4 follows the differential rotation of a Solar-type star. The profiles of specific entropies are as follows: Q_0 is constant across the flow, Q_1 varies from Q_0 to $Q_0/2$ and Q_2 varies from Q_0 to zero like Q_1 but more smoothly in the latter case. More details about the definitions of these functions are given in an appendix of Paper I.

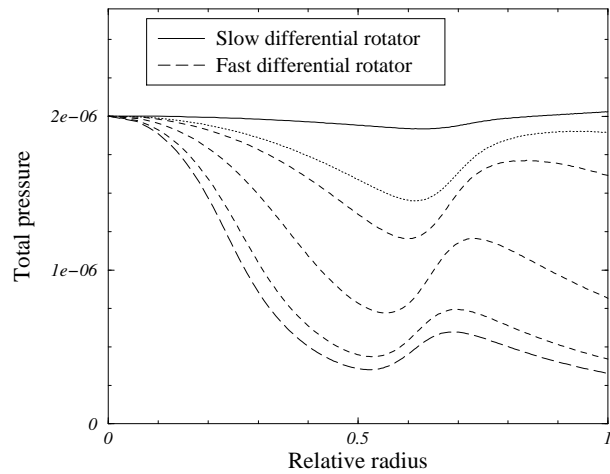


Fig. 11. Plots of the total pressure for a differential rotator as a function of the relative radius r_{rel} for different central values of the rotation rate. The angular velocity $\Omega(a)$ (type Ω_2 varies from its maximum value Ω_0 on the axis to half of it ($\Omega_0/2$) at the middle of the total radius of the jet ($r_* = \frac{r}{r_{jet}} = 0.5$) with a smooth step like profile (See Paper I for exact profile definition). Slow rotators are represented with solid lines and fast differential rotators with dashed lines.

A number of well-collimated outflows are observed to have larger poloidal velocities near the polar axis, and lower velocities at the edge of the flow. This motivated us to use a profile of type Ω_2 that could reproduce such behaviors. Fig.(11) represents the total pressure for such differential rotators with respect to the relative radius for a set of central values of the angular velocity. Similarly to rigid rotators, the pressure globally decreases from the axis to the outer edge, though the gradient of rotation causes a second peak of pressure to appear. For slow and intermediate rotators, the inner pressure can be of order of the pressure at boundary of the jet and the outer part can be as dense and slow as the axial region. A peak of poloidal velocity accompanies the pressure minimum which produces a double structure in such outflows, with a dense slow core surrounded by a faster component at half of the

part of the jet has the maximum momentum. Differential rotators can then produce jets with a narrow central part with large momentum surrounded by a larger outflow with a lesser momentum, as are jet surrounded by a molecular flow.

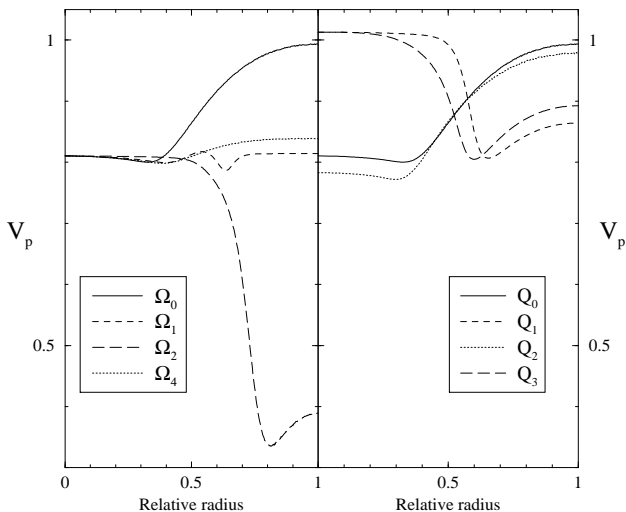


Fig. 12. Poloidal velocity profiles across the flow. Left panel illustrates differential rotators. Ω_0 correspond to constant rotation rate. Ω_1 and Ω_2 go from a maximum value on the axis to zero and half of this maximum on the equator respectively. Ω_4 present a Solar-like differential rotation. Right panel shows differential entropies. Q_0 is correspond to constant Q across the outflow. Q_1 has a step-like profile from 1 to 0.5. Q_2 goes from a maximum value on the axis to zero on the equator (idem for Q_3 but more smoothly)

In Fig.(12) the poloidal velocity is plotted as a function of the relative radius for various differential rotation and entropy profiles. Some outflows like rigid rotators have smaller axial velocities than at the outer edge or present on the contrary a very fast component which corresponds to large gradients of the angular velocity. Differential entropies can also cause such inverted asymptotic solutions though with less amplitude in the variation of the poloidal velocity.

Variations of the entropy profile bring an interesting feature. We have shown previously that magnetic pressure dominates at the outer edge for fast rotators while gas pressure dominates for slow rotators. A varying specific entropy can enhance this difference as shown in Fig.(13) where total, gas and magnetic pressures are plotted with respect to the relative radius. The total pressure does not change much as compared to the case of constant entropy while the magnetic to gas pressure ratio increases. In the

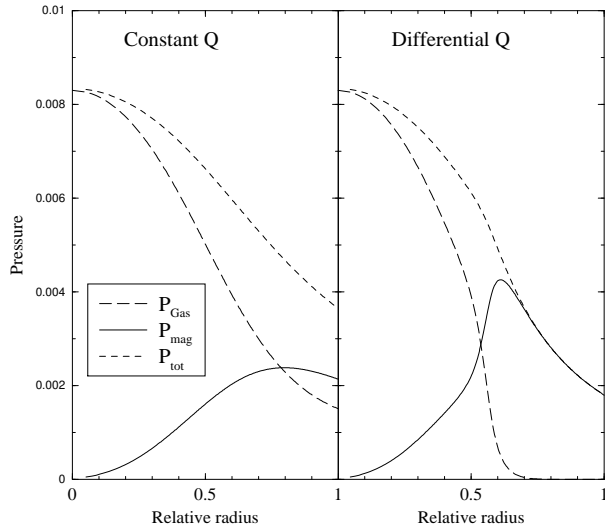


Fig. 13. Effects of differential specific entropy. Comparison of asymptotic solutions of magnetic (solid), gas (long dashed) and total (dotted) pressures for constant (left) and differential (right) specific entropies. Parameters correspond to a fast rotator. The angular velocity $\bar{\Omega}$ is constant.

5. The asymptotic electric current

Heyvaerts and Norman (1989) have shown that the asymptotic shape of steady axisymmetric magnetized unconfined outflows is either paraboloidal or cylindrical according to whether the electric current carried at infinity vanishes or not. As shown in previous sections, the uniform confining external pressure causes the flow to asymptote to a cylindrical shape. The aim of this section is to study the variation of the poloidal electric current in our solutions as the confining pressure is reduced to zero. We will find a relation between the current, the axial density and the external pressure and will investigate how the currents vary with the input parameters and with the rotation profile.

The physical poloidal current through a circle centered on the axis of symmetry and flowing between this axis and a magnetic surface a is given by

$$I_{phys}(a) = \frac{2\pi r B_\phi}{\mu_0} \quad (26)$$

The related, usually positive quantity $I = -I_{phys}/2\pi$, which we will still refer to as the "poloidal electric current" therefore contains entirely equivalent information. Let us define the following dimensionless variables normalized to their value at the Alfvén surface:

$$x = \frac{r^2}{r_A^2} \quad \text{and} \quad y = \frac{\rho}{\rho_A}, \quad (27)$$

the energy parameter

$$\epsilon \equiv \frac{2E}{v_{PA}^2} \quad (29)$$

the gravity parameter

$$g \equiv \frac{2GM}{r_A v_{PA}^2}. \quad (30)$$

The value of the flux surface index, a , at the equator corresponds to the total magnetic flux enclosed in the outflow and is defined by

$$A = \int_0^{\pi/2} B R^2 \cos \theta d\theta. \quad (31)$$

We make the magnetic flux dimensionless by dividing it by A :

$$a_* = \frac{a}{A}. \quad (32)$$

In terms of these variables the poloidal current can be written, by equation (9) which is valid for $r \gg r_A$, as

$$I = \frac{A}{\mu_0 r_A} \omega x y \quad (33)$$

It has been found convenient to first consider constant values of $\Omega(a)$ and $Q(a)$ to investigate the dependence of the electric current on model parameters and on the external confining pressure. Non constant profiles for rotation and specific entropy will be considered later on.

5.1. Current and pressure balance

In the dimensionless variables x and y defined above the equations for the asymptotic structure of the flow are written as

$$\left(\frac{dx}{da_*} + \frac{2x}{r_A} \frac{dr_A}{da_*} \right)^2 = \frac{4}{y^2 (\epsilon - \beta y^{\gamma-1} - 2\omega^2 x y)} \quad (34)$$

$$\left(\frac{\gamma-1}{\gamma} \right) x r_A^2 \frac{d}{da_*} \left(\frac{\beta y^\gamma}{r_A^4} \right) + \frac{d}{da_*} \left(\frac{\omega^2 x^2 y^2}{r_A^2} \right) = 0 \quad (35)$$

Considering that the variation of the position of the Alfvén point with respect to the relative magnetic flux is small, the Bernoulli equation (equation 34) can be written as

$$\dot{x} = \frac{dx}{da_*} = \frac{2}{y \sqrt{\epsilon - \beta y^{\gamma-1} - 2\omega^2 x y}}. \quad (36)$$

Assuming $\Omega(a)$ and $Q(a)$ to be constant, the transfield equation similarly reduces to

$$\dot{y} = \frac{dy}{da_*} = -y \left(\frac{2\omega^2 \dot{x}}{(\gamma-1) \beta y^{\gamma-2} + 2\omega^2 x} \right) \quad (37)$$

where C is an integration constant which can be expressed in terms of the value of the mass density on the axis $y(x=0) = y_0$ as

$$C = \beta y_0^{\gamma-1} \quad (39)$$

Equation (38) gives, using equation (33), the value of the total poloidal asymptotic electric current as:

$$I = \frac{A}{2r_A \mu_0} \frac{\beta}{\omega} (y_0^{\gamma-1} - y_b^{\gamma-1}) \quad (40)$$

The values of both y_0 and y_b , the latter corresponding to the relative density at the outer boundary, are part of the solution. The condition for a vanishing asymptotic current is simply $y_0 = y_b$ in the case of a non-vanishing entropy. The next step is to find a relation between the external pressure and the densities involved in equation (40). The transfield equation (37) can be reformulated in differential form and, making use of the definition of its integration constant C in equation (38), can be cast in the equivalent form:

$$\dot{y} = - \frac{2\omega^2 y^2 \dot{x}}{(\gamma-2) \beta y^{\gamma-1} + C} \quad (41)$$

and the Bernoulli equation is simply

$$\dot{x} = \frac{2}{y \sqrt{\epsilon - C}} \quad (42)$$

Substituting \dot{x} from equation (42) in equation (41) we obtain

$$\dot{y} \left((\gamma-2) \beta y^{\gamma-2} + \frac{C}{y} \right) = - \frac{4\omega^2}{A \sqrt{\epsilon - C}} \quad (43)$$

that can be integrated between the axis and the outer edge of the outflow (y varies from y_0 to y_b and a varies from 0 to 1):

$$C \ln \left(\frac{y_b}{y_0} \right) + \frac{\beta(\gamma-2)}{\gamma-1} (y_b^{\gamma-1} - y_0^{\gamma-1}) = - \frac{4\omega^2}{\sqrt{\epsilon - C}} \quad (44)$$

Pressure balance at the outer edge of the jet gives a relation between the external pressure and the axial density:

$$\tilde{P}_{ext} = \frac{\gamma-1}{\gamma} \beta y_b^\gamma + \omega^2 x_b y_b^2 + y_b^2 (\epsilon - \beta y_b^{\gamma-1} - 2\omega^2 x_b y_b) \quad (45)$$

where \tilde{P}_{ext} is defined by

$$\tilde{P}_{ext} \equiv \frac{2\mu_0 r_A^4}{A^2} P_{ext}. \quad (46)$$

Then the pressure balance equilibrium reduces to

$$\tilde{P}_{ext} = \frac{\gamma-1}{\gamma} \beta y_b^\gamma + \omega^2 x_b y_b^2 + y_b^2 (\epsilon - C) \quad (47)$$

The system of equations (45) and (44) establishes a relation between the external pressure \tilde{P}_{ext} and the axial

5.1.1. Slow rotators

In the previous section (see Fig. (3)), it has been shown that, for slow rotators, gas pressure is larger than magnetic pressure at the outer boundary. One can easily understand that since $\omega \ll 1$. In this case, it is equivalent to

$$\tilde{P}_{ext} = \frac{\gamma-1}{\gamma} \beta y_b^\gamma \gg \epsilon - C \quad (48)$$

Since the energy parameter ϵ has been calculated for slow rotators in Paper I and is given by $\epsilon = 1 + \beta + 3\omega^2 - g$, equation (48) is given by

$$y_b = \left(\frac{\gamma \tilde{P}_{ext}}{(\gamma-1)\beta} \right)^{1/\gamma} \quad (49)$$

In fact g has been neglected with respect to β as a first approximation. Using equations (5.1.1), (39) and (49), the equation (44) becomes

$$\begin{aligned} \frac{1}{\gamma} \ln \left(\frac{\gamma \tilde{P}_{ext}}{(\gamma-1)\beta y_0^\gamma} \right) + \left(\frac{\gamma-2}{\gamma-1} \right) \left(\frac{\gamma \tilde{P}_{ext}}{(\gamma-1)\beta y_0^\gamma} \right)^{\frac{\gamma-1}{\gamma}} \\ = - \frac{4\omega^2}{\beta y_0^{\gamma-1} \sqrt{1 + \omega^2 - \beta(1 + y_0^{\gamma-1})}} + \frac{\gamma-2}{\gamma-1} \end{aligned} \quad (50)$$

The second terms of both the left and right hand sides are negligible with respect to the first terms and this equation can be simplified to:

$$\tilde{P}_{ext} = \frac{\gamma-1}{\gamma} \beta y_0^\gamma \exp - \frac{4\omega^2 \gamma}{\beta y_0^{\gamma-1} \sqrt{1 + \omega^2 - \beta(1 + y_0^{\gamma-1})}} \quad (51)$$

Since β and ω have been obtained by a solution for the inner part of the flow close to the source, this equation is a relation between the external pressure and the asymptotic axial density. It is now possible to calculate the poloidal current as a function of the density on the axis:

$$I \approx \frac{\gamma-1}{2\mu_0 r_A} \frac{\beta y_0^\gamma}{\omega} \left(1 - \exp \left(- \frac{4\omega^2 \gamma}{\beta y_0^{\gamma-1}} \right) \right) \quad (52)$$

All other parameters in this formula are given by the solution in the inner part of the flow close to the source and by the boundary condition on the axis. So equations (51) and (52), give a relation between the external pressure and the total poloidal current in the slow rotator case.

5.1.2. Fast rotators

In the case of fast rotators, we have seen that the gas pressure is negligible with respect to the magnetic pressure

Using equation (45) and condition (53), equation (44) becomes now

$$\begin{aligned} \frac{C}{2} \ln \left(\frac{\tilde{P}_{ext}}{\epsilon - C} \right) - \frac{C}{\gamma-1} \ln \left(\frac{C}{\beta} \right) \\ - \frac{\beta(\gamma-2)}{(\gamma-1)} \left(\frac{\tilde{P}_{ext}}{\epsilon - C} \right)^{\frac{\gamma-1}{2}} - \frac{\gamma-2}{\gamma-1} C = - \frac{4\omega^2}{\sqrt{\epsilon - C}} \end{aligned} \quad (54)$$

It has two simple solutions, when the external pressure becomes small, which are $C \sim 0$ and $C \sim \epsilon \approx 3\omega^{\frac{4}{3}}$. In the latter case the corresponding poloidal current is given by:

$$I = \frac{A}{2r_A \mu_0 \omega} \left(3\omega^{4/3} - \beta y_b^{\gamma-1} \right) \quad (55)$$

and if either β or the relative density at the boundary is small compared to unity, it reduces to

$$I = \frac{3}{2} \frac{A}{r_A \mu_0} \omega^{1/3} \quad (56)$$

It has been shown in paper I that the Alfvén radius grow with ω faster than $\omega^{1/3}$ for fast rotators. Then the current I decreases as the rotator gets faster and the fast rotator does not carry the largest electric current among the different possible magnetic rotators. When ω approaches its limit $\left(\frac{3}{2}\right)^{\frac{3}{2}}$ corresponding to the very fast rotator the current approaches

$$I = \left(\frac{3}{2} \right)^{3/2} \frac{A}{r_A \mu_0} \quad (57)$$

Since r_A has been found in paper I to be proportional to $\alpha^{-1/3}$, the total current increases with α .

5.2. Variation of the current across the flow

Using the equations obtained previously, it is also possible to investigate the variation of the asymptotic poloidal current across the jet. Differentiating the current as given by equation (33) with respect to a we find

$$\begin{aligned} \frac{dI}{da_*} &= \frac{2A\omega}{r_A \mu_0 \sqrt{\epsilon - C}} \left(1 + \frac{2\omega^2 x y^2}{\beta(\gamma-1)y^\gamma} \right)^{-1} \\ &= \frac{2A\omega}{r_A \mu_0 \sqrt{\epsilon - C}} \left(1 + \frac{4}{\gamma} \frac{P_{B\phi}}{P_{gas}} \right)^{-1} \end{aligned} \quad (58)$$

Along the same lines as above, we can study the slow rotator case where the gas pressure dominates and the fast rotator case which has a strong magnetic pressure at the outer edge. In the former case, one finds that

$$\frac{dI}{da_*} = \frac{2A\omega}{r_A \mu_0 \sqrt{\epsilon - C}}$$

The slope of the variation of the poloidal current tends to vanish as ω decreases. It is proportional to $\frac{\omega}{r_A}$. For slow rotators the derivative is always positive and then the current is diffuse in the outflow. For fast rotators the magnetic pressure dominates, $C = \beta y_0^{-1} \ll \epsilon$ and one has

$$\begin{aligned} \frac{dI}{da_*} &= \frac{A\omega\gamma}{2r_A\mu_0\sqrt{\epsilon}} \frac{P_{gas}}{P_{B_\phi}} \\ &\sim \frac{A\omega^{1/3}\gamma}{2\sqrt{3}r_A\mu_0} \frac{P_{gas}}{P_{B_\phi}} \end{aligned} \quad (60)$$

The magnitude of the slope $\frac{dI}{da_*}$ tends to vanish for very fast rotators since the gas to magnetic pressure ratio decreases with the rotation parameter. In the latter case the slope approaches small values more rapidly than in the slow rotator case. Another interesting point is that the gas to magnetic pressure ratio starts to decrease very rapidly at a small value of the distance r to the axis, so its derivative goes rapidly to zero across the jet as a function of radius. This means that all the current must be enclosed in a core around the axis for fast rotators, which should carry concentrated electric current.

5.3. Evolution of the current along the flow

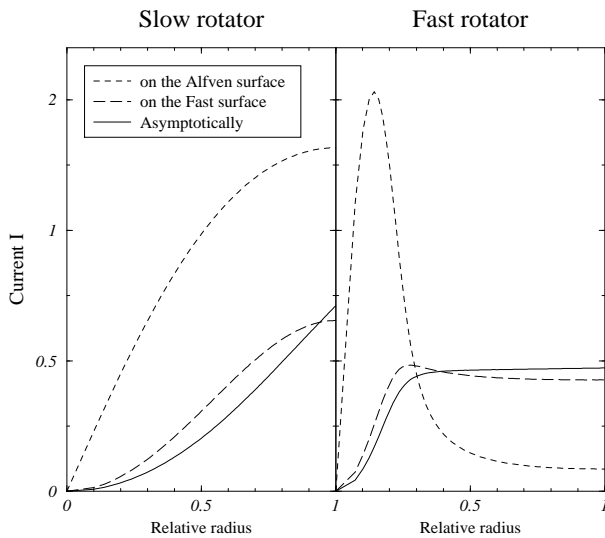


Fig. 14. Variations of the current along the flow for slow (left panel) and fast (right panel) rotators as functions of the relative radius $r_{rel} = \frac{r}{r_{jet}}$. The electric current is calculated in the asymptotic region (solid lines), at the Alfvén surface (dashed lines) and at the fast magnetosonic surface (long dashed lines).

surface, at the fast surface and asymptotically are plotted with respect to the relative radius $r_{rel} = \frac{r}{r_{jet}}$, which is almost linearly related to $a_{rel} = a/A$ with a slope equal to unity. The left panel stands for slow rotators while the right panel shows the currents for fast rotators. For slow rotators, the poloidal electric current globally decreases from the Alfvén surface to the asymptotic zone, but is constantly increasing from the polar axis to the edge of the jet. On the other hand the right panel shows that the current at the Alfvén surface has a peak close to the polar axis for fast rotators. The current then decreases at larger distances from the axis which reveals the existence of a return electric current flowing around the central electric flow. This illustrates that the solutions obtained with this model carry return currents at other locations than at the polar axis, contrary to self-similar models. The total current decreases and vanishes at infinity. Essentially all of the current is located in the first third of the total radius. This agrees with our earlier conclusion in this section, fast rotators have a concentrated current around the polar axis while slow rotators carry a diffuse current.

5.4. Influence of source properties

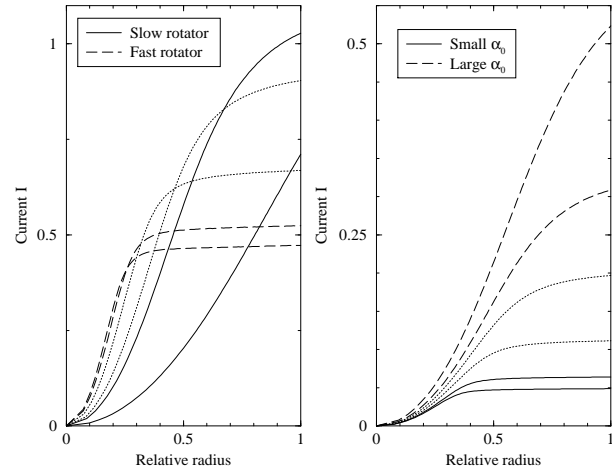


Fig. 15. Plots of the asymptotic electric current profile for different values of constant angular velocity $\bar{\Omega}$ (left panel) and of the mass to magnetic flux ratio on the axis $\bar{\alpha}_0$ (right panel). Heavy solid lines correspond to slow rotators (left panel) and to small $\bar{\alpha}_0$ (right panel), while fast rotators (left panel) and large $\bar{\alpha}_0$ are plotted with heavy long dashed lines. Thin dashed lines correspond to intermediate values.

The parameters whose changes produce the strongest variations of the solutions are the angular velocity $\bar{\Omega}$ and the mass to magnetic flux ratio on the axis $\bar{\alpha}_0$. The left

creases but soon starts to decrease. The maximum current does not correspond to the largest rotation rate. On the right panel of Fig.(15), the current is plotted for different values of $\bar{\alpha}_0$ for a given $\bar{\Omega}$. The larger the mass to magnetic flux ratio, the more the properties of the outflow resemble those of a slow rotator. The current profile changes from a concentrated one, signature of a fast rotator, to a more diffuse one for the largest $\bar{\alpha}_0$. The total current increases at the meantime. So jets with large mass loss rate also possess a large current.

5.5. Influence of the external pressure

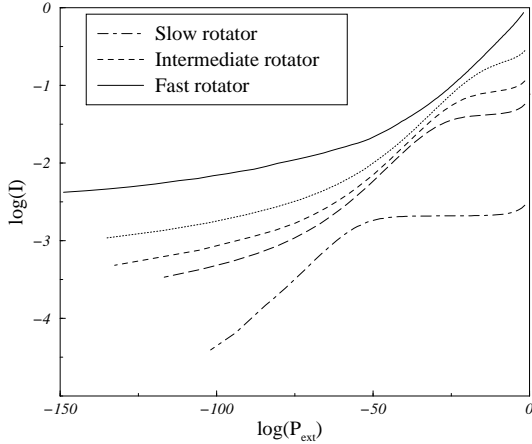


Fig. 16. Plots of the asymptotic electric current with respect to the external confining pressure for various types of rigid rotators. The solid lines correspond to the fastest rotators while the dashed lines stand for slow rotators. $\bar{Q} = 3.1$, $\bar{\alpha}_0 = 2.5$ and $\bar{\Omega}$ varies from 0.1 to 15 corresponding to ω varying from 0.1 to 1.8. Note that the lower limits of the external pressure correspond to extremely large radii of the outflows.

At the edge of the asymptotic region, the outflow is in pressure equilibrium with the surrounding external medium. There is a relation between the total current and this pressure. We plot in Fig.(16) the total asymptotic poloidal current in the jet as a function of the confining pressure for different types of rotators ranging from slow to very fast ones. All other parameters are kept constant. The curves are stopped at a very small value of the external pressure which causes the radius of the jet to have become larger than any reasonable astronomical size for them, in fact as large as the radius of the visible universe.

The total current diminishes as the external pressure drops for all types of rotators but never approaches a constant non-vanishing limit when the pressure is decreased

but it strongly decreases for smaller ones. For very fast rotators the current varies little with external pressure.

It would have been interesting to reach a conclusion on whether the asymptotic poloidal current vanishes or not in the limit of vanishing confining pressures. This issue is important because it distinguishes the different possible asymptotic regimes for unconfined jets (Heyvaerts and Norman, 1989). Fig.(18) does not show any leveling-off of the current I as $\log P_{ext}$ approaches $-\infty$. Conversely, even though extremely small pressures have been considered, it remains dubious, except perhaps for the very slow rotator, whether such asymptote will ever be reached. Regardless of the smallness of the limiting values of the pressure that have been reached, this study does not allow to conclude that the current vanishes when the pressure rigorously does. However, from a practical point of view, it appears that a significant residual current remains, even for exceedingly small, but non-vanishing, confining pressure.

5.6. Differential rotators

In previous parts of this section, analytical solutions for the current have been given when angular velocity is assumed to be constant across the flow. We now investigate the case when the gradient of angular velocity with respect to the magnetic flux a is large compared to the variation of the radius x and of the specific entropy Q . In this case, $\dot{\omega} \gg \dot{x}$, and equation (37) can be written as

$$\dot{y} = -\frac{2xy^2\omega\dot{\omega}}{(\gamma-1)\beta y^{\gamma-1} + 2\omega^2 xy} \quad (61)$$

which is equivalent to

$$(\gamma-1)\beta y^{\gamma-1}\dot{y} + 2\omega^2 xy^2 \left(\frac{\dot{y}}{y} + \frac{\dot{\omega}}{\omega} \right) = 0 \quad (62)$$

In this case the transfield equation can be integrated neglecting the relative derivative of the radius with respect to the relative derivatives of the density and of the rotation parameter. The integral is:

$$\frac{\gamma-1}{\gamma}\beta y^{\gamma} + \omega^2 xy^2 = C_2 \quad (63)$$

where C_2 is a constant of integration which can be expressed in terms of the density on the axis as

$$C_2 = \beta y_0^{\gamma-1} \quad (64)$$

Equation (63) can be transformed using equation (33) into an equation for the current, that we will note I_{diff} , the solution of which is:

$$I_{diff} = \frac{A}{r_A \mu_0} \frac{\gamma-1}{\gamma} \frac{\beta}{\omega y_b} \left(y_0^{\gamma-1} - y_b^{\gamma-1} \right) \quad (65)$$

This is different from the solution for the rigid rotator case, that can be noted I_{rigid} . The relation between them

This shows that the total current for differential rotators with large gradients of angular velocity will be larger since the density on the boundary is small compared to unity. This can clearly be seen in the left panel of Fig.(17) where the current is plotted with respect to the radius for different types of differential rotators. The largest values of the current correspond to profiles where the gradients of the angular velocity are positive and are the largest, namely for profiles of type Ω_2 , where the angular velocity takes half of its value at the middle of the outflow.

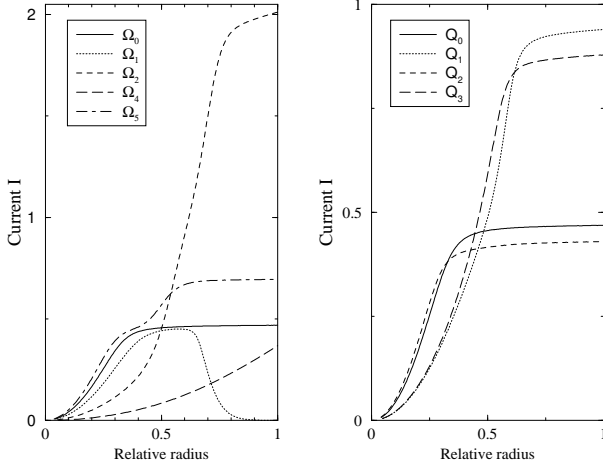


Fig. 17. Plots of the electric current profiles across the flow with respect to the relative radius $r_{rel} = \frac{r}{r_{jet}}$. Left panel stands for differential angular velocities and right panel shows differential specific entropies. Variations of the surface functions $\Omega(a)$ and $Q(a)$ are the same than those given in Fig.(12). Note the difference of ranges between different panels.

On the other hand the solution obtained with an angular velocity vanishing on the outer edge of the flow (type Ω_1) gives a poloidal current that decreases drastically and vanishes close to the boundary. This reveals the presence of a large return current at the outer part of the outflow. Fig.(17) shows that the profile of the angular velocity is also of prime importance. The variation of entropy with flux have a lesser influence on the current profile.

6. Comparison between numerical results and a simplified model

In a review of the theory of magnetically accelerated outflows and jets from accretion disks, Spruit (1994) discusses the asymptotic wind structure. Following the same method as in paper I we use his method and find that

The net current from this simplified analytical model, that we will note I_{simp} , is defined by equation. (33), so:

$$I_{simp} = \frac{\omega A x y}{\mu_0 r_A} = \frac{\omega A}{\mu_0 r_A} \left(1 - \left(\frac{\alpha}{\alpha_* \omega} \right)^{4/3} \left(\frac{r_A}{r_*} \right)^2 \right) \quad (68)$$

which can be written as a function of the mass to magnetic flux ratio α as

$$I_{simp} = \frac{9\omega A}{5\mu_0 r_*} \left(\frac{\alpha}{\alpha_*} \right)^{1/3} \left(1 - \left(\frac{5\alpha}{9\alpha_* \omega^2} \right)^{2/3} \right) \quad (69)$$

Thus this current is proportional to the angular velocity and the mass loss rate with the following dependencies

$$I_{simp} \propto \Omega \dot{M}^{1/3} \quad (70)$$

The current can also be given as a function of the rotation parameter ω and of the Alfvén radius by

$$I_{simp} \approx \frac{3\omega^{1/3} A}{2\mu_0 r_A} \quad (71)$$

We have plotted this analytical solution with respect to ω in Fig.(18) together with the numerical result. The agreement between the two is good for small values of the rotation parameter. As ω increases and passes 0.5, the two solutions separate in the intermediate rotator region to converge again in the limit of very fast rotators. As shown previously the current increases with respect to ω for slow rotators and diminishes in the other limit. So the analytical results we have found for the current are in qualitative agreement with the real value.

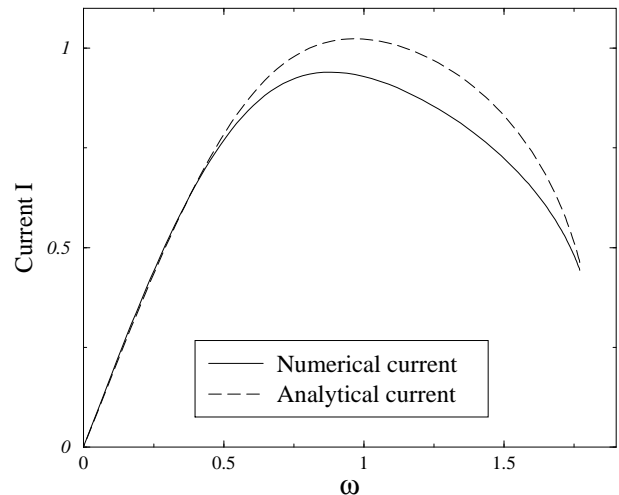


Fig. 18. Comparison of numerical results (solid line) and analytical solutions (dashed line) of the asymptotic electric current I with respect to the rotation parameter ω .

It is also interesting to calculate the Poynting flux per

Using our dimensionless variables it can be expressed as

$$S = \frac{A^2}{\mu_0 \rho_A r_A^4} \omega^2 xy = \frac{A}{\rho_A r_A^3} I \omega \quad (73)$$

The Poynting flux using the above simplified analytical results is given by

$$S_{simp} = \frac{A^2}{\mu_0 \rho_A r_A^4} \frac{3}{2} \omega^{4/3} = v_{pA}^2 \frac{3}{2} \omega^{4/3} \quad (74)$$

Other formulation with respect to ω and α using the previous equation (69) for I_{simp} and replacing it in equation (73) for S , we have

$$S_{simp} = \frac{A}{\rho_A r_A^3} \frac{9\omega^2 A}{5\mu_0 r_*} \left(\frac{\alpha}{\alpha_*} \right)^{1/3} \left(1 - \left(\frac{5\alpha}{9\alpha_* \omega^2} \right)^{2/3} \right) \quad (75)$$

which scales with the rotation and mass loss rate as

$$S_{simp} \propto \frac{\Omega^2}{\dot{M}^{2/3}} \quad (76)$$

This analytical solution is plotted with respect to the relative radius together with the numerical results with the same input parameters. The agreement is quite good all across the outflow. So equation (75) represents well the behavior of the asymptotic Poynting flux.

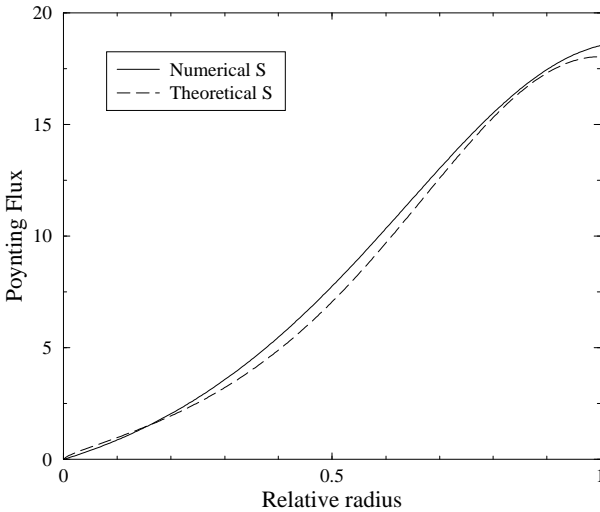


Fig. 19. Comparison of numerical results (solid line) and analytical solutions (dashed line) for the Poynting flux S across the outflow as functions of the relative radius $r_{rel} = \frac{r}{r_{jet}}$.

The wind carries both kinetic and magnetic energy, the asymptotic ratio of these, at large distance, is a measure of the importance of the magnetic component. The kinetic

and the Poynting to kinetic energy flux ratio is given by

$$q = \frac{S}{K} = \frac{3\omega^{4/3}}{\rho} \frac{v_{pA}^2}{v_p^2} \quad (78)$$

The effects of the external pressure on the Poynting to kinetic energy fluxes ratio q have been calculated for the different classes of rotators. It is found that the faster the rotator, the larger the ratio q which increases with the confining pressure. In the case of slow rotators, the ratio is smaller than unity while it is larger for fast rotators.

In paper I, it has been shown that a general constraint applies on the solution in terms of two physical quantities, the Poynting flux S and the specific enthalpy H at the slow and fast surfaces

$$[S^2 H]_{slow} \geq [S^2 H]_{fast} . \quad (79)$$

If the fast surface goes to infinity for the very fast rotator limiting case, the Poynting flux calculated at the fast surfaces coincide with the asymptotic one that we have just calculated. Using equations (75) and (79) a new constraint can be given for the boundary mass density ρ_b

$$(\rho_b)_\infty \leq \frac{\rho_A r_A^3}{A} \frac{5\mu_0 r_*}{9\omega^2 A} \left(\frac{\alpha_*}{\alpha} \right)^{1/3} \frac{[S^2 \rho^{\gamma-1}]_{slow}}{1 - \left(\frac{5\alpha}{9\alpha_* \omega^2} \right)^{2/3}} \quad (80)$$

Thus the asymptotic density at the outer edge of the outflow has an upper bound in terms of quantities defined in the inner part of the outflow close to its source. This upper bound given by equation (80) for the axial mass density could be used as a constrain for initial conditions of numerical simulations.

7. Conclusions

We have considered the asymptotic behavior of outflows of magnetized rotators confined by an external uniform pressure in the framework of our simplified model. The asymptotic forms of transfield and Bernoulli equations were used to determine the jet structure taking into account the pressure balance across the interface between the flow and the external confining medium. No self-similar assumption has been made. The given confining pressure has been regarded as a boundary condition and the constants of the motion obtained in the inner part of the flow close to the emitting source have been used. The full range of possible variations of the parameters has been explored.

Slow rotators are dominated by thermal effects from the axis to the outer edge. The specific entropy however has little influence on their asymptotic magnetic field.

In the case of fast rotators rotational and mass loss rate effects have the most important influences on so-

gradients asymptotically. A large part of the magnetic energy is not transferred to the kinetic energy and the outflow is strongly magnetized asymptotically and carries a significant Poynting flux.

Whatever the type of rotator, isothermal jets are narrower than adiabatic ones under the same conditions. The densest jets are slower on the boundary than lighter ones. In the case of slow rotators, an analytical solution for the current in terms of the axial density, thermal and rotation parameters has been obtained. This relation combined with the analytical solution gives the asymptotic current as a function of the confining pressure. An analytical solution for the poloidal current has also been obtained in the case of the fast rotator in terms of the rotation parameter and the Alfvén radius. The current in slow rotators is diffuse in the outflow while fast rotators carry a concentrated electric current around the axis. The solutions obtained with our model can carry return currents out of the polar axis, contrary to self-similar models. The comparison between numerical results and approximate analytic solutions show the latter to be good qualitative estimators of the real value.

Non constant profiles of rotation and, to a lesser extent of entropy, cause the solutions to change drastically. For example, the largest asymptotic poloidal velocity can be located either on the axis or at the outer edge according to the profile of $\Omega(a)$. It has been possible to find solutions resembling observed flows such as central jets with important momentum surrounded by a larger outflow. Large currents can be generated by differential rotators if the gradient of the angular velocity is large and the angular velocity does not vanish on the outer edge of the flow.

Thus our model makes it possible to relate the properties of the asymptotic part of an outflow to those of the source. Our calculated asymptotic equilibria can be useful in investigating the propagation of jets and the instabilities that can develop in magnetized outflows. They can be used as input conditions for MHD simulation codes. Instabilities presently under study are likely to be important in such asymptotic equilibria.

Acknowledgements. We would like to thank Kanaris Tsinganos for his remarks as referee that helped to clarify some of the derivations and discussions of equations.

References

- Appl S., Camenzind C., 1993, A&A 274, 699
 Bertout, C., et al., 1988, ApJ, 330, 350
 Blandford, R.D., Payne, D.G., 1982, MNRAS, 199, 883
 Chan, K.L., Henriksen, R.N., 1980, ApJ, 241, 534
 Contopoulos, J., Lovelace, R.V.E., 1994, ApJ, 429, 139
 Ferreira, J., Pelletier, G., 1993a, A&A, 276, 625
 Ferreira, J., Pelletier, G., 1993b, A&A, 276, 637
 Goodson, A., Winglee, R., Boehm, K., 1997, ApJ, 489, 199
 Henriksen, R.N., Valls-Gabaud, D., 1994, MNRAS, 266, 681
 Heyvaerts, J., Norman, C., 1989, ApJ, 347, 1055
 Heyvaerts, J., 1996, *Plasma Astrophysics* eds. Chiuderi, C., Einaudi, G., (Springer), 31
 Lery, T., Heyvaerts, J., Appl, S., Norman, C.A., 1998, A&A, 337, 603
 Li, Z. Y., Chiueh, T., Begelman, M.C., 1992, ApJ, 394, 459
 Li, Z. Y., 1995, ApJ, 444, 848
 MacGregor, K., B., 1996, in *Solar and Astrophysical MHD flows*, K. Tsinganos (ed.), Kluwer Academic Publishers, 301
 Ouyed, R., Pudritz, R., 1997, ApJ, 482, 712
 Pelletier, G., Pudritz, R.E., 1992, ApJ, 394, 117
 Sauty, C., Tsinganos, K., 1994, A&A, 287, 893
 Shu, F.H., Lizano, S. Ruden, S.P. and Najita, J. 1988, ApJ, 328, L19
 Shu, F.H., Najita, J., Ostriker, E., Wilkin, F., Ruden, S. and Lizano, S., 1994, ApJ, 429, 781
 Spruit, H.C., 1994, *Cosmical Magnetism*, NATO ASI Series C. eds. D. Lynden-Bell (Kluwer), 422, 33
 Trussoni, E., Tsinganos, K., Sauty, C., 1997, A&A, 325, 1099
 Tsinganos, K., Sauty, C., 1992, A&A, 255, 405
 Tsinganos, K., Trussoni, E., 1991, A&A, 249, 156
 Tsinganos, K., Sauty, C., Surlantzis, G., Trussoni, E., Contopoulos, J., 1996, in *Solar and Astrophysical MHD flows*, K. Tsinganos (ed.), Kluwer Academic Publishers, 379
 Weber, E.J., Davis, L., 1967, ApJ, 148, 217